RSC Advances

This is an *Accepted Manuscript*, which has been through the Royal Society of Chemistry peer review process and has been accepted for publication.

Accepted Manuscripts are published online shortly after acceptance, before technical editing, formatting and proof reading. Using this free service, authors can make their results available to the community, in citable form, before we publish the edited article. This *Accepted Manuscript* will be replaced by the edited, formatted and paginated article as soon as this is available.

You can find more information about *Accepted Manuscripts* in the Information for Authors.

Please note that technical editing may introduce minor changes to the text and/or graphics, which may alter content. The journal's standard Terms & Conditions and the Ethical guidelines still apply. In no event shall the Royal Society of Chemistry be held responsible for any errors or omissions in this *Accepted Manuscript* or any consequences arising from the use of any information it contains.

ROYAL SOCIETY OF CHEMISTRY

www.rsc.org/advances

Please do not adjust margins

RSC Advances

ARTICLE

Smooth $CH_3NH_3PbI_3$ from controlled solid-gas reaction for photovoltaic applications

Received 00th January 20xx,
Accepted 00th January 20xx

DOI: 10.1039/x0xx00000x

www.rsc.org/

Jian Mao,[a] Hong Zhang,[a] Hexiang He,[b] Haifei Lu,[a] Fengxian Xie,[a] Di Zhang,[a] Kam Sing Wong,[b] and Wallace C. H. Choy[a*]

The merit of high power conversion efficiency (PCE) and easy preparation makes organic-inorganic perovskite solar cell as one of the most promising solar devices. However, the PCE is greatly dependent on the morhpolgy of perovskite thin film. Here, we report a solid-gas reaction method to fabricate quite smooth $CH_3NH_3PbI_3$ thin film with high coverage. Through controlling the reaction rate between CH_3NH_3I and PbI_2 by tunning PbI_2 substrate temperature and evaporation rate of CH_3NH_3I, we obtain $CH_3NH_3PbI_3$ layer with roughness of 7.37 nm. Besides, no post-treatment of annealing is needed after the film formation for our approach. With about 250 nm perovskite active layer, the solar cells exhibits a PCE of 10.0% with little hysteresis.

1. Introduction

As one of the emerging and globally investigated solar cells, three-dimensional organic-inorganic perovskite has intrigued remarkable attention in recent years for its high absorption coefficient from 300 nm to 800 nm (1.5×10^4 cm^{-1} at 550 nm)[1,2], long exciton diffusion length (1 micrometer for polycrystal[3] and 175 micrometers for single crystal[4]), easy solution process[5,6,7], and low cost[8]. The general chemical formula of perovskite is ABX_3 (A = CH_3NH_3 or $HC(NH_2)_2$, B = Pb or Sn, and X = Cl, Br, or I). Through simply varying the elements of A, B, and X, the band gap of perovskite can be easily tuned from 1.3 eV[9] to 2.3 eV[10] for wide band absorption of sunlight. With the considerably increasing power conversion efficiency (PCE)[6], perovskite solar cells (PSCs) are highly potential to approach the theoretical maximum efficiency of 33.7% as for single p-n junction solar cell , which was theoretically predicted when the band gap of absorber material was about 1.34 eV[11].

The study of three-dimensional organic-inorganic perovskite dated back to several decades ago[12, 13], however not until recently has it been applied in solar cells. In 2006, Kojima and co-workers[14] utilized $CH_3NH_3PbBr_3$ perovskite as sensitizer in solar cells and reported a PCE of 2.19%. After several years research, the certificated efficiency of perovskite solar cells has been improved to 20.1%[15]. Despite the exciting progress, there are still some challenges to be overcome for practical applications of PSCs. For example, repeatability and stability of perovskite solar cell are not very good. The anomalous hysteresis[16] dependent on scan direction and scan rate of applied voltage to perovskite solar cells is also a concern. Besides, it is quite difficult to prepare perovskite thin film with full coverage[17]. In conventional one-step solution coating method, perovskite precursor is prepared from mixture of CH_3NH_3I and PbI_2[2] or CH_3NH_3I and $PbCl_2$[3] in solvent of Dimethylformamide (DMF)[6, 18, 19], or Gamma-butyrolactone (GBL)[20, 21]. The easily obtained morphology with incomplete coverage[19, 22-25] might be related to the solvent-induced intermediates[26] of $CH_3NH_3PbI_3{\cdot}DMF$ and $CH_3NH_3PbI_3{\cdot}H_2O$ as well as colloidal nature[27] of precursor in solvent with size ranging from tens nanometers to micrometers. On the other hand, dual-source vapor deposition[22, 28] without the usage of solvent has been reported to offer quite smooth perovskite thin film with very good coverage. However, the device performance from this approach is very sensitive to the evaporation rates of the two sources. More recently, vapor-assisted solution process (VASP)[29] has been developed. While this approach needs a relatively high temperature (150 °C) to sublimate CH_3NH_3I powder and anneal perovskite thin film. Fabrication of efficient perovskite solar cells at low temperature with smooth morphology and complete coverage is desired.

Herein, we report a solid-gas reaction method to fabricate $CH_3NH_3PbI_3$ thin film. The evaporated CH_3NH_3I molecule interacts upon contact with solid PbI_2 spin coated on substrate at 60 °C under vacuum and leads to compact and smooth thin film with high coverage. No extra annealing is needed after formation of the film. Besides, we find that the solid-gas reaction of PbI_2 and CH_3NH_3I at room temperature is very slow and occurs only at the surface of PbI_2. Nevertheless, the PbI_2 substrate heated to 60 °C can completely convert PbI_2 into $CH_3NH_3PbI_3$. This can be explained by the improved diffusion rate of CH_3NH_3I molecules within PbI_2 layer and the increased

[a] Department of Electrical and Electronic Engineering, The University of Hong Kong ,Pok Fu Lam Road, Hong Kong, China. E-mail: chchoy@eee.hku.hk
[b] Department of Physics, The Hong Kong University of Science & Technology, Clear Water Bay, Kowloon, Hong Kong, China.

RSC Advances Accepted Manuscript

Please do not adjust margins

reaction rate between the solid PbI_2 and gaseous CH_3NH_3I at higher temperature. By optimizing the substrate temperature, CH_3NH_3I evaporation rate, and PbI_2 thickness, we obtain perovskite thin film of about 250 nm, which gives PCE of 10.0% with little hysteresis.

2. Experimental

2.1 Materials

Lead (II) iodide (PbI_2, 99.9%), N, N-Dimethylformamide (DMF, anhydrous, 99.8%), and Chlorobenzene (CB, 99.8%) were purchased from Sigma Aldrich. Isopropanol (IPA, anhydrous, 99.8%) was bought from Acros Organics. PEDOT:PSS (P VP AI 4083) was purchased from Clevios. $PC_{61}BM$ was purchased from Solarmer Energy Inc. Poly[(9,9-bis(3'-(N,N-dimethylamino) propyl)-2,7-fluorene)-alt-2,7-(9,9-dioctylfluorene)] (PFN) was purchased from 1-Material. Methylammonium iodide (CH_3NH_3I) was synthetized by reacting 13.5 ml Methylamine (CH_3NH_2, 33wt% in ethanol, Sigma Aldrich) and 15 ml hydroiodic acid (HI, 57wt% in water, Sigma Aldrich) under ice bath for 2 hours. White precipitate was obtained by removing solvent with rotary evaporator at 55 °C. The precipitate was purified by recrystallization process which started with dissolving the precipitate in ethanol and followed by adding excess diethyl ether to get precipitate again. The process was repeated for three times. After recrystallization, the precipitate was dried at 60 °C for 24 hours in vacuum.

2.2 Device preparation

The perovskite solar cells have a structure of ITO/ PEDOT:PSS (40 nm)/ $CH_3NH_3PbI_3$ (150-250 nm)/ $PC_{61}BM$ (50 nm)/ PFN (1-2 nm)/ Ag (120 nm). ITO substrate was washed successively with deionized water, acetone, and ethanol. After UVO treatment, ITO substrate was spin coated with PEDOT:PSS at 4000 rpm for 40 s and annealed at 130 °C for 15 min. PbI_2 was dissolved in DMF with concentration of 300 mg/ml, 462 mg/ml, and 550 mg/ml and stirred at 60 °C for more than 10 hours before use. Yellow PbI_2 precursor was spin coated on PEDOT:PSS at 5000 rpm for 10 s and immediately dried at 90 °C for 15 min(300 mg/ml leads to about 60 nm, 462 mg/ml leads to about 100 nm, and 550 mg/ml leads to about 130 nm). After drying, the samples were mounted on sample holder and then put into vacuum chamber. The PbI_2 side of sample was facing down to CH_3NH_3I source. The distance between sample and CH_3NH_3I source was fixed approximate to 30 cm. Besides, the volume of vacuum chamber was about 58000 cm^3. The chamber pressure was controlled at 10^{-4} Pa and the metal sample holder was heated to the desired temperatures of 50 °C, 60 °C, and 70 °C with stability of ± 1 °C. The density of CH_3NH_3I was assumed as 1 $g.cm^{-3}$, as reported by Snaith[22]. The evaporation rate was controlled at 0.5 Å/s, 0.9 Å/s, and 1.3 Å/s via tuning the evaporation current and recorded using Maxtek Model TM-400. After evaporation for 60-80 min, the excess CH_3NH_3I was washed with IPA. $PC_{61}BM$ (20 mg/ml in CB) was spin coated atop at 1500 rpm, followed by PFN (0.2 mg/ml in ethanol) at coating rate of 3000 rpm. Finally, 120 nm Ag was evaporated on PFN at vacuum pressure of 3×10^{-4} Pa.

2.3 Characterization

Simulated AM 1.5 sun light (100 mW/cm^2) was generated by ABET AM 1.5G solar simulator and calibrated by Hamamatsu silicon reference cell. The current density-voltage curve of $CH_3NH_3PbI_3$ solar cells was recorded using Keithley 2635 SourceMeter. Incident photon to current efficiency (IPCE) was performed with home-built system combining a Newport xenon lamp, an Acton monochromator, and a chopper with a Stanford lock-in amplifier. High resolution Scanning Electron Microscope (SEM) images were obtained from LEO 1530 FEG SEM. Before SEM measurement, 5 nm gold was evaporated on $CH_3NH_3PbI_3$

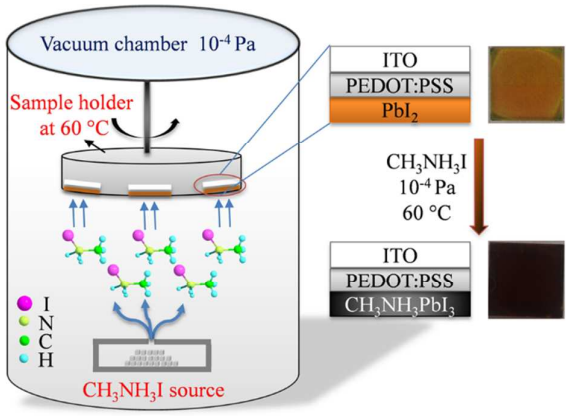

Fig. 1 Schematic image of $CH_3NH_3PbI_3$ formation via solid-gas reaction at low temperature under vacuum.

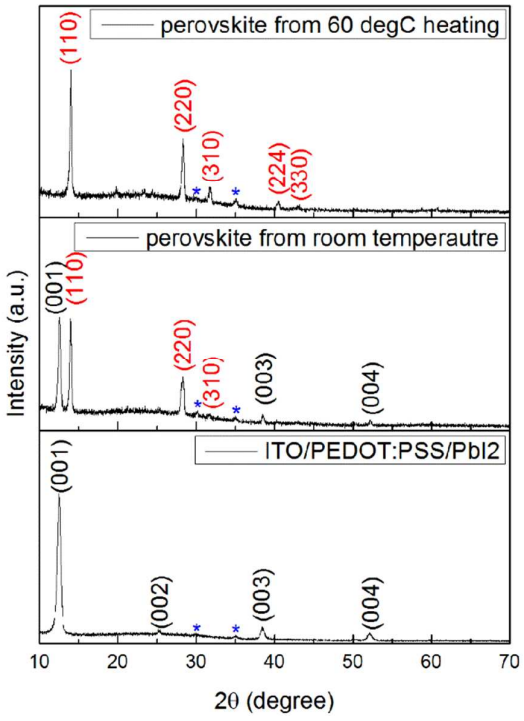

RSC Advances Accepted Manuscript

This journal is © The Royal Society of Chemistry 20xx

Fig. 2 XRD spectrum of PbI_2 on ITO/PEDOT:PSS, perovskite on ITO/PEDOT:PSS from room temperature, and perovskite on ITO/PEDOT:PSS from substrate at 60 °C. The peaks marked with blue asterisk at 30.27° and 35.08° were assigned to ITO (PDF#39-1058).

thin film. X-ray Diffraction (XRD) spectrum was measured with Empyrean model from PANanalytical equipped with anode material of Cu (k-alpha, λ = 1.540598 Å). The generator voltage and current were 40 kV and 40 mA respectively. Atomic Force Microscopy (AFM) was performed using Bruker Veeco Multimode V in trapping mode.

3. Results and discussion

Figure 1 shows the schematic image of formation of $CH_3NH_3PbI_3$ thin film via solid-gas reaction at low temperature under vacuum. Details of the operation conditions can be found in Experimental Section. The evaporated CH_3NH_3I molecules react with heated PbI_2 upon contact and result in the formation of $CH_3NH_3PbI_3$, which can be preliminarily judged by the color change of thin film from yellow to dark brown.

When the substrate temperature is at room temperature, we observe that PbI_2 substrate after evaporation of excess CH_3NH_3I is not dark brown but yellow. However after heating substrate to 60 °C during the evaporation, the evaporated device becomes dark brown. XRD spectra show the crystalline properties of the PbI_2 on substrate, perovskite from evaporation of CH_3NH_3I at room temperature and 60 °C, as plotted in Figure 2. The peaks at 30.27° and 35.08°, marked with blue asterisk, exist in all devices and are assigned to ITO (PDF#39-1058). Peaks at 12.52°, 25.35°, 38.44°, and 52.12° are observed in the PbI_2 samples before CH_3NH_3I evaporation which are attributed to PbI_2 crystal (PDF#07-0235), corresponding to (001) (002), (003), and (004) lattice phases, respectively. After the evaporation of excess CH_3NH_3I at room temperature and the wash by isopropanol (IPA), peaks at 12.52°, 38.44°, and 52.12° still exist. Besides, new peaks at 14.03°, 28.27°, and 31.74° are observed and assigned to the characteristic peaks of $CH_3NH_3PbI_3$[30], which means the evaporated samples at room temperature are mixture of PbI_2 and $CH_3NH_3PbI_3$. On the other hand, for the evaporated samples annealed at 60 °C during evaporation, all peaks assigned to PbI_2 disappear, indicating complete conversion of PbI_2 into $CH_3NH_3PbI_3$. This phenomenon should attribute to increased diffusion rate of CH_3NH_3I in PbI_2 layer and increased reaction rate between CH_3NH_3I and PbI_2 at higher temperature. After getting energy from heated substrate, CH_3NH_3I molecules with increased kinetic energy can easily diffuse throughout the PbI_2 layer. On the other hand, in terms of chemical kinetics, the reaction rate between CH_3NH_3I and PbI_2 (as descried by equation 1) is a function of rate constant, reactants' concentration, as shown in equation 2.

$$PbI_{2\,(s)} + CH_3NH_3I_{\,(g)} \leftrightarrow CH_3NH_3PbI_{3\,(s)} \quad (1)$$

$$\nu = \kappa[CH_3NH_3I]^a[PbI_2]^b \quad (2)$$

where ν is reaction rate, κ is rate constant, $[CH_3NH_3I]$ is mole concentration of CH_3NH_3I, a is order in CH_3NH_3I, $[PbI_2]$ is mole concentration of PbI_2, and b is order in PbI_2.

Following Arrhenius equation, the rate constant κ is dependent on temperature

$$\kappa = Ae^{-E_a/RT} \quad (3)$$

where A is constant, E_a is activation energy of reaction, R is universal gas constant, and T is temperature.

Referring to equations (2) and (3), when the temperature is uplifted, the rate constant κ increases, and thus the reaction rate ν raises. Besides, this result also indicates that the reaction between CH_3NH_3I and PbI_2 is endothermic.

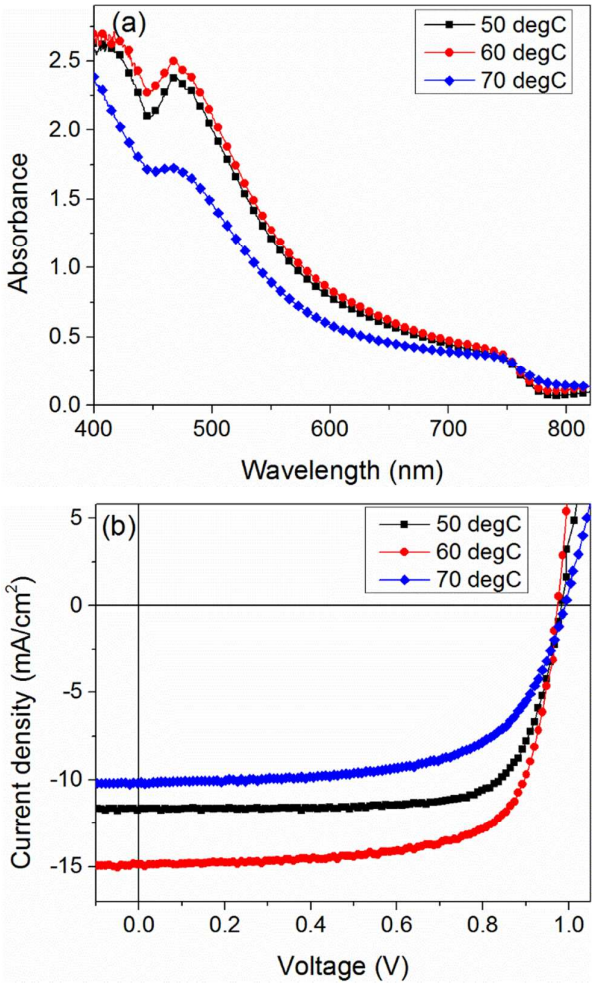

Fig. 3 a) Absorbance of $CH_3NH_3PbI_3$ thin films and b) J-V characteristics of $CH_3NH_3PbI_3$ solar cells prepared from substrate at 50 °C, 60 °C, and 70 °C.

3.1 Effects of substrate temperature on perovskite thin film

Substrate temperatures of 50 °C, 60 °C, and 70°C during evaporation of CH_3NH_3I have been investigated. By studying the absorption spectra of the perovskite film as shown in Figure 3(a), we find that absorption of perovskite augments with increasing substrate temperature from 50 °C to 60 °C, which means crystallization quality of the formed perovskite is better at higher temperature. However, when the substrate temperature is further increased to 70 °C, the absorption

RSC Advances Accepted Manuscript

decreases. Besides, the color of the perovskite film becomes lighter than perovskite prepared at the substrate temperatures of 50 °C and 60 °C. Two reasons might account for this result.

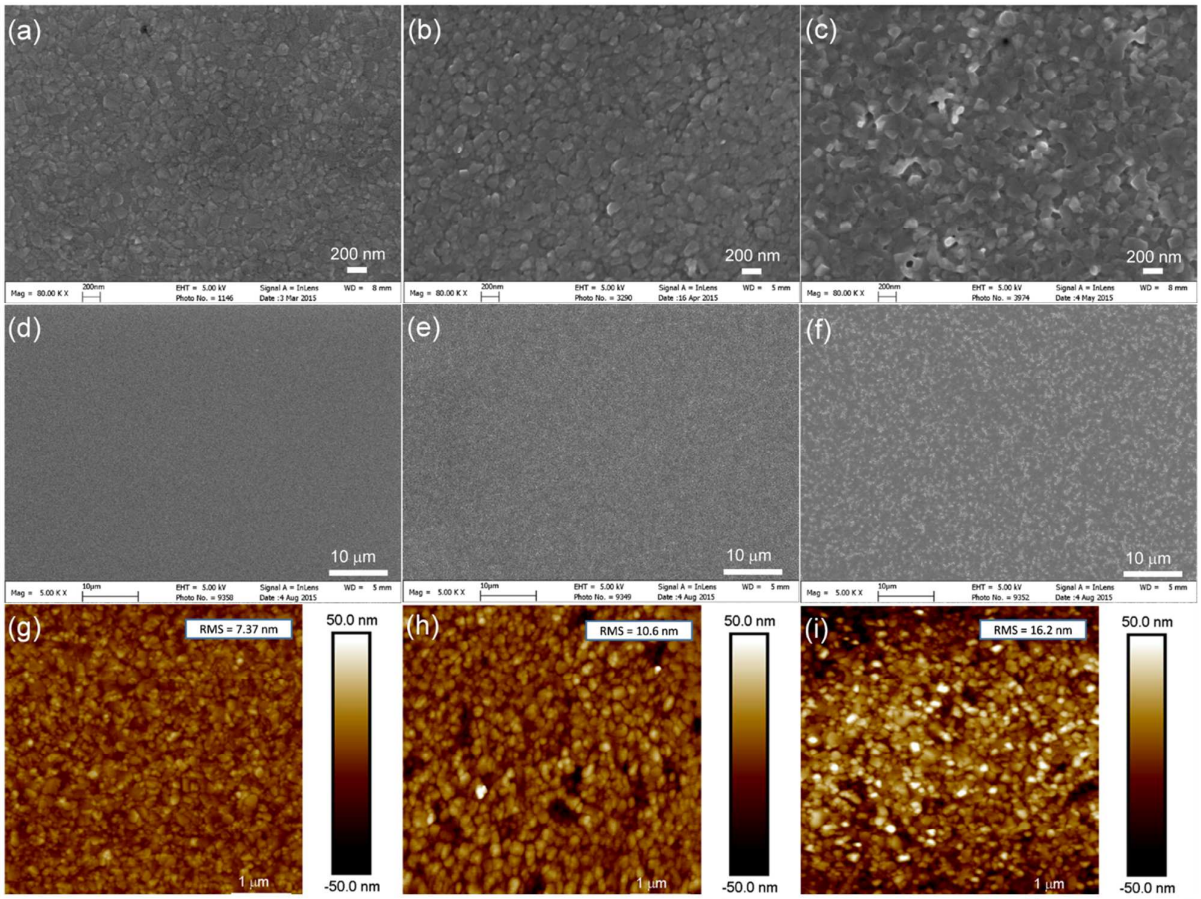

Fig. 4 a) High resolution SEM image, d) Low resolution SEM image, and g) AFM image of perovskite thin film from the CH_3NH_3I evaporation rate of 0.5 Å/s. b) High resolution SEM image, e) Low resolution SEM image, and h) AFM image of perovskite thin film from the CH_3NH_3I evaporation rate of 0.9 Å/s. c) High resolution SEM image, f) Low resolution SEM image, and i) AFM images of the perovskite films from the CH_3NH_3I evaporation rate of 1.3 Å/s. The size of AFM image is 5 μm × 5 μm.

First, when the temperature is further increased to higher temperature and reaches 70°C, it could favour the backward reaction in the reversible reaction[31,32] (equation 1). In this case, the decomposition rate of $CH_3NH_3PbI_3$ might increase and less perovskite will form (and thus the color will become lighter). Another possible reason is that it is thermodynamically unfavorable for CH_3NH_3I molecules to deposit on hot PbI_2 substrate with temperature of 70°C. The major evaporated CH_3NH_3I molecules are either evacuated away or deposit on cold chamber wall. Accordingly, the formation of perovskite is hindered. Similar phenomenon of degraded perovskite film at much higher temperature is also observed in the reaction between $PbCl_2$ and CH_3NH_3I[33]. The reduced absorbance of perovskite thin film prepared from substrate temperature of 70 °C is accompanied with decreased PCE of the corresponding solar cells, specifically decreased short-circuit current density (J_{sc}). Figure 3b shows the current density- voltage of perovskite solar cells from substrate at 50 °C, 60 °C, and 70 °C. The PCE increases from 8.37% (J_{sc} = 11.38 mA/cm^2) to 10.00% (J_{sc} = 14.65 mA/cm^2) but decreases to 6.33% (J_{sc} = 10.18 mA/cm^2) with increasing substrate temperature from 50 °C to 70 °C.

3.2 Effects of CH_3NH_3I evaporation rate on perovskite film

Based on equation (2), the reaction rate between PbI_2 and CH_3NH_3I depends on the concentration of CH_3NH_3I, so we change the concentration of CH_3NH_3I by controlling the evaporation rate of CH_3NH_3I and the optimized substrate temperature is 60 °C. Evaporation rates of 0.5 Å/s, 0.9 Å/s, and 1.3 Å/s have been investigated. Figure 4 shows the Scanning Electron Microscope (SEM) and Atomic Force Microscopy (AFM) images of the perovskites prepared from different CH_3NH_3I evaporation rates. SEM shows that the average diameter of perovskite crystal size increases slightly with increasing evaporation rate. This increased crystal sized might be attributed to improved forward reaction rate of PbI_2 and CH_3NH_3I. Besides, the roughness (Rq) of perovskite films from CH_3NH_3I evaporation rate of 0.5 Å/s, 0.9 Å/s, and 1.3 Å/s are 7.37 nm, 10.6 nm, and 16.2 nm, respectively. The increased roughness under higher evaporation rate might be due to uneven nucleation rate.

RSC Advances Accepted Manuscript

This journal is © The Royal Society of Chemistry 20xx

Deposited CH_3NH_3I reacts with surface PbI_2 and leads to primary nucleation of $CH_3NH_3PbI_3$. At a higher evaporation rate, more amount of CH_3NH_3I will present at surface of PbI_2, which favours the secondary nucleation of $CH_3NH_3PbI_3$ on the primary sites. The nucleic sites of big crystal size might grow at higher rate for its larger contact area. As a result, the big crystal will grow even larger while the growth of nucleic site of small crystal is diminished. Accordingly, the roughness is enhanced. Nevertheless, under low evaporation rate, the nucleation rate for formation of perovskite seeds is quite

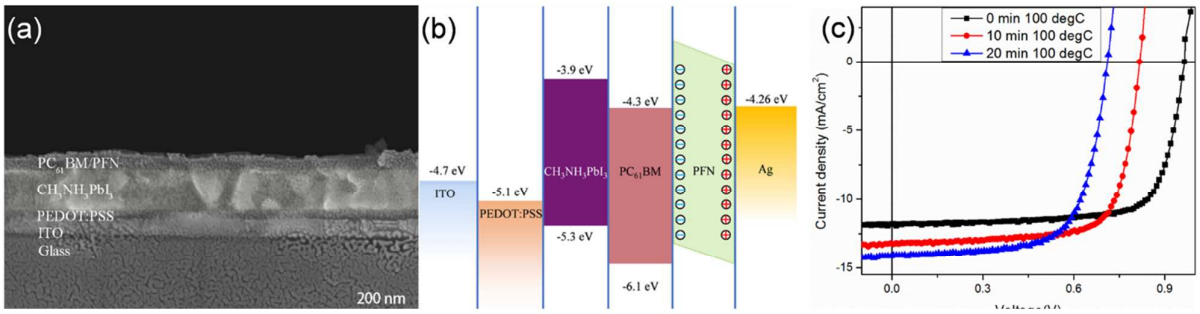

Fig. 5 a) Cross-sectional SEM image of pervoskite solar cell. b) Energy level diagram of the solar cell with structure of *ITO/ PEDOT:PSS (40 nm)/ $CH_3NH_3PbI_3$ (250 nm)/ $PC_{61}BM$ (50 nm)/ PFN (1-2 nm)/ Ag (120 nm).* c) Current density voltage curves of perovskite solar cell after 0 min, 10 min, and 20 min post-annealing of perovskite thin films at 100 °C.

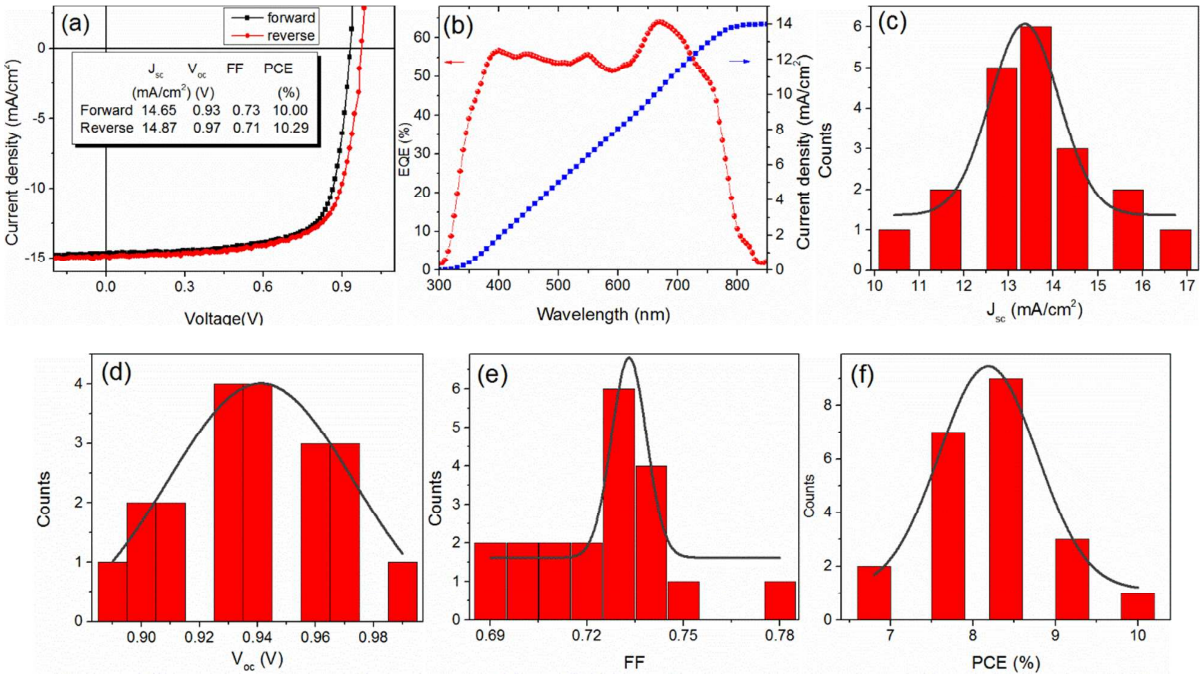

Fig. 6 a) Current density-voltage curve and b) Incident photon to current efficiency (IPCE) of $CH_3NH_3PbI_3$ solar cells. c) J_{sc}, d) V_{oc}, e) FF, and f) PCE histograms of 20 samples.

uniform over the substrate because no extra CH_3NH_3I presents at surface and new evaporated CH_3NH_3I almost equally deposits at each nucleic site. Indeed, the roughness of the evaporation rate of 0.5 Å/s is even smaller than that (8.3 nm) of the one with the highest certificated perovskite solar cells[34]. On the other hand, lower CH_3NH_3I evaporation rate of 0.1-0.2 Å/s has been investigated. However, we find that the color of device after evaporation of CH_3NH_3I for more than two hours is slightly brown, which means small amount perovskite forms. Perovskite solar cell with this thin film exhibits very poor performance (less than 1%). We attribute the result to too slow reaction rate between PbI_2 and CH_3NH_3I. Lower CH_3NH_3I evaporation rate leads to lower concentration of CH_3NH_3I. Too low concentration of CH_3NH_3I diminishes the chance of effective collision between gaseous CH_3NH_3I molecules and PbI_2. According to collision theory[35], effective collision is the premise for two compounds to react with each other. As a result, the formation of perovskite under such condition is quite difficult.

3.3 Perovskite film from PbI_2 with different thicknesses

We have prepared 60 nm and 100 nm thick PbI_2 films via spin coating its precursor with concentration of 300 mg/ml and 462 mg/ml in DMF, respectively. After evaporation of

RSC Advances Accepted Manuscript

excess CH_3NH_3I with rate of 0.5 Å/s and substrate temperature at 60 °C. The formed perovskite are measured to be about 150 nm and 250 nm using Step Profiler. With these perovskite active layers, the corresponding solar cells exhibit PCEs of 6.49% and 10.0%, respectively (SI1). However, we fail to prepare even thicker perovskite from 130 nm PbI_2 (from 550 mg/ml PbI_2 in DMF). Though we evaporate all of the CH_3NH_3I (1.5 g) that can be stored in our source boat, the conversion of PbI_2 into perovskite is not complete, resulting in lower absorption of perovskite thin film and poor performance of solar cell (less than 2%). We attribute the result to too large volume of our vacuum chamber (approximate 58000 cm^3). The utilization of evaporated CH_3NH_3I in such big chamber is very low. Most of the CH_3NH_3I are deposited on the cold wall or evacuated away.

3.4 Photovoltaic performance after post-annealing

The photovoltaic characterization is investigated after making 250 nm perovskite film into solar cells. The cross-section SEM image of the cell is shown in Figure 5a. PEDOT:PSS and $PC_{61}BM$ works as hole transporting layer and electron transporting layer, respectively. PFN[36] is used as dipole between $PC_{61}BM$ and silver cathode to facilitate electron transport. The corresponding energy diagram is shown in Figure 5b. Post-annealing of deposited perovskite thin film at 100 °C has been investigated. Figure 5c shows the J-V curve of perovskite solar cells from 100 °C annealing of perovskite thin film for 0 min, 10 min, and 20 min. The J_{sc} of perovskite solar cells increases with increasing annealing time, which can be explained by improved crystallization of perovskite thin film. However, it should be noticed that 100 °C annealing even for 10 min would reduce the V_{oc} and FF. This phenomenon has also been reported by Ziqi Liang and co-workers[37]. The drop of V_{oc} might be due to increased non-radiative recombination centres under annealing at 100 °C[38, 39].

3.5 Optimized device performances

The champion device without post-annealing has a PCE of 10.0%, J_{sc} of 14.65 mA/cm^2, V_{oc} of 0.93 V, and FF of 0.73 (as shown in Figure 6a). The J_{sc} matches well with the value (14.01 mA/cm^2) by integrating IPCE, as shown in Figure 6b. The histograms of J_{sc}, V_{oc}, FF, and PCE of 20 samples are displayed in figure 6c-f. It can be seen that the average PCE is more than 8%. Compared with reported high performance $CH_3NH_3Pb(I,Cl)_3$ solar cell[7, 40, 41] which contains more than 400 nm active layer, the lower PCE and especially lower short-circuit current of perovskite solar cell from our approach are mostly attributed to thinner perovskite layer. So large vacuum chamber (approximate 58000 cm^3) in our lab makes the utilization of evaporated CH_3NH_3I very low, leading to incomplete conversion of thick PbI_2 into perovskite even after evaporating all of CH_3NH_3I that can be stored in source boat. As a result, thick perovskite is hard to get under current condition. However, this issue should not be a problem for vacuum chamber with small volume and large source boat. The hysteresis which occurs in most perovskite devices[42-44] is also investigated in our device. The scan rate of our device is 0.13 V/s, which is slight lower than usually reported 0.15 V/s[42]. It is generally accepted that hysteresis is more severe at lower scan rate[16]. Our results are shown in Figure 6a. It can be seen that PCEs of our device are very close under forward (PCE = 10.0%) and reverse scan (PCE = 10.3%), which indicates that the hysteresis in our device is very small.

Conclusions

In summary, a solid-evaporated gas reaction method has been developed to fabricate $CH_3NH_3PbI_3$ perovskite solar cells with very smooth morphology and high coverage. No post-treatment of annealing is needed after the film formation for our approach. The smooth morphology originates from the slow reaction of solid PbI_2 and diluted gas CH_3NH_3I molecule and uniform nucleation rate. Compared with traditional one-step or two-step methods where solvent-induced intermediates might account for the complete coverage, our approach avoids the usage of solvent during film preparation and results in high coverage. The PCE of 10.0% and little hysteresis have been obtained in our device. Consequently, the work contribute to development of low temperature and simple approaches for fabricating perovskite solar cells.

Acknowledgements

This study is supported by the University Grant Council of the University of Hong Kong (grant 201311159056), the General Research Fund (grants HKU711813 and HKU711612E), the Collaborative Research Fund (grant C7045-14E) and RGC-NSFC grant (N_HKU709/12) from the Research Grants Council of Hong Kong Special Administrative Region, China, and grant CAS14601 from CAS-Croucher Funding Scheme for Joint Laboratories. K.S. would like to acknowledge the financial support of AoE/P-02/12 the Research Grants Council. We thank Paddy K. L. Chan and Zhichao Zhang for help of AFM measurement.

Notes and references

1. J. H. Im, C. R. Lee, J. W. Lee, S. W. Park and N. G. Park, *Nanoscale*, 2011, 3, 4088-4093.
2. H. S. Kim, C. R. Lee, J. H. Im, K. B. Lee, T. Moehl, A. Marchioro, S. J. Moon, R. Humphry-Baker, J. H. Yum, J. E. Moser, M. Gratzel and N. G. Park, *Sci. Rep.*, 2012, 2, 591.
3. S. D. Stranks, G. E. Eperon, G. Grancini, C. Menelaou, M. J. Alcocer, T. Leijtens, L. M. Herz, A. Petrozza and H. J. Snaith, *Science*, 2013, 342, 341-344.
4. Y. F. Q. Dong, Y. Shao, P. Mulligan, J. Qiu, L. Cao, J. Huang, *Science*, 2015.

RSC Advances Accepted Manuscript

This journal is © The Royal Society of Chemistry 20xx

5. J. Burschka, N. Pellet, S. J. Moon, R. Humphry-Baker, P. Gao, M. K. Nazeeruddin and M. Gratzel, *Nature*, 2013, 499, 316-319.
6. H. Zhou, Q. Chen, G. Li, S. Luo, T. B. Song, H. S. Duan, Z. Hong, J. You, Y. Liu and Y. Yang, *Science*, 2014, 345, 542-546.
7. J. H. Im, I. H. Jang, N. Pellet, M. Gratzel and N. G. Park, *Nat. Nanotechnol.*, 2014, 9, 927-932.
8. H. J. Snaith, *J. Phys. Chem. Lett.*, 2013, 4, 3623-3630.
9. F. Hao, C. C. Stoumpos, D. H. Cao, R. P. H. Chang and M. G. Kanatzidis, *Nat. Photonics*, 2014, 8, 489-494.
10. J. H. Noh, S. H. Im, J. H. Heo, T. N. Mandal and S. I. Seok, *Nano Lett.*, 2013, 13, 1764-1769.
11. W. Shockley and H. J. Queisser, *J. Appl. Phys.*, 1961, 32, 510.
12. D. Weber, *Z. Naturforsch.* , 1978, 33b, 1443.
13. A. Poglitsch and D. Weber, *J. Chem. Phys.*, 1987, 87, 6373-6378.
14. K. T. A. Kojima, T. Miyasaka, Y. Shirai, presented in part at the 210th ECS Meeting, 2006.
15. http://www.nrel.gov/ncpv/images/efficiency_chart.jpg.
16. H. J. Snaith, A. Abate, J. M. Ball, G. E. Eperon, T. Leijtens, N. K. Noel, S. D. Stranks, J. T. W. Wang, K. Wojciechowski and W. Zhang, *J. Phys. Chem. Lett.*, 2014, 5, 1511-1515.
17. G. E. Eperon, V. M. Burlakov, P. Docampo, A. Goriely and H. J. Snaith, *Adv. Funct. Mater.*, 2014, 24, 151-157.
18. P. Docampo, J. M. Ball, M. Darwich, G. E. Eperon and H. J. Snaith, *Nat. Commun.*, 2013, 4, 2761.
19. J. Y. Jeng, Y. F. Chiang, M. H. Lee, S. R. Peng, T. F. Guo, P. Chen and T. C. Wen, *Adv. Mater.*, 2013, 25, 3727-3732.
20. K. T. K. Kojima, Y. Shirai, T. Miyasaka, *J. Am. Chem. Soc.*, 2009, 131, 6050.
21. L. Etgar, P. Gao, Z. Xue, Q. Peng, A. K. Chandiran, B. Liu, M. K. Nazeeruddin and M. Gratzel, *J. Am. Chem. Soc.*, 2012, 134, 17396-17399.
22. M. Liu, M. B. Johnston and H. J. Snaith, *Nature*, 2013, 501, 395-398.
23. Q. Wang, Y. C. Shao, Q. F. Dong, Z. G. Xiao, Y. B. Yuan and J. S. Huang, *Energ Environ. Sci.*, 2014, 7, 2359-2365.
24. W. Ke, G. Fang, J. Wan, H. Tao, Q. Liu, L. Xiong, P. Qin, J. Wang, H. Lei, G. Yang, M. Qin, X. Zhao and Y. Yan, *Nat. Commun.*, 2015, 6, 6700.
25. B. Conings, L. Baeten, C. De Dobbelaere, J. D'Haen, J. Manca and H. G. Boyen, *Adv. Mater.*, 2014, 26, 2041-2046.
26. F. Hao, C. C. Stoumpos, Z. Liu, R. P. Chang and M. G. Kanatzidis, *J. Am. Chem. Soc.*, 2014, 136, 16411-16419.
27. K. Yan, M. Long, T. Zhang, Z. Wei, H. Chen, S. Yang and J. Xu, *J. Am. Chem. Soc.*, 2015, 137, 4460-4468.
28. O. Malinkiewicz, A. Yella, Y. H. Lee, G. M. Espallargas, M. Graetzel, M. K. Nazeeruddin and H. J. Bolink, *Nat. Photonics*, 2013, 8, 128-132.
29. Q. Chen, H. P. Zhou, Z. R. Hong, S. Luo, H. S. Duan, H. H. Wang, Y. S. Liu, G. Li and Y. Yang, *J. Am. Chem. Soc.*, 2014, 136, 622-625.
30. A. Mei, X. Li, L. Liu, Z. Ku, T. Liu, Y. Rong, M. Xu, M. Hu, J. Chen, Y. Yang, M. Gratzel and H. Han, *Science*, 2014, 345, 295-298.
31. Q. Chen, H. P. Zhou, T. B. Song, S. Luo, Z. R. Hong, H. S. Duan, L. T. Dou, Y. S. Liu and Y. Yang, *Nano letters*, 2014, 14, 4158-4163.
32. Y. Jin and G. Chumanov, *Chem Lett*, 2014, 43, 1722-1724.
33. C. W. Chen, H. W. Kang, S. Y. Hsiao, P. F. Yang, K. M. Chiang and H. W. Lin, *Adv. Mater.*, 2014, 26, 6647-6652.
34. N. J. Jeon, J. H. Noh, Y. C. Kim, W. S. Yang, S. Ryu and S. I. Seok, *Nat. Mater.*, 2014, 13, 897-903.
35. J. d. P. Peter Atkins, *Physical Chemistry*, 2006.
36. F. X. Xie, D. Zhang, H. Su, X. Ren, K. S. Wong, M. Gratzel and W. C. Choy, *ACS nano*, 2015, 9, 639-646.
37. Y. N. Chen, Y. X. Zhao and Z. Q. Liang, *Chemistry of Materials*, 2015, 27, 1448-1451.
38. W. Tress, N. Marinova, O. Inganäs, M. K. Nazeeruddin, S. M. Zakeeruddin and M. Graetzel, *Adv. Energy Mater.*, 2015, 5, n/a-n/a.
39. J. Yao, T. Kirchartz, M. S. Vezie, M. A. Faist, W. Gong, Z. He, H. Wu, J. Troughton, T. Watson, D. Bryant and J. Nelson, *Phys. Rev. Appl.*, 2015, 4.
40. W. Y. Nie, H. H. Tsai, R. Asadpour, J. C. Blancon, A. J. Neukirch, G. Gupta, J. J. Crochet, M. Chhowalla, S. Tretiak, M. A. Alam, H. L. Wang and A. D. Mohite, *Science*, 2015, 347, 522-525.
41. N. Ahn, D. Y. Son, I. H. Jang, S. M. Kang, M. Choi and N. G. Park, *J. Am. Chem. Soc.*, 2015, 137, 8696-8699.
42. W. Zhang, M. Saliba, D. T. Moore, S. K. Pathak, M. T. Horantner, T. Stergiopoulos, S. D. Stranks, G. E. Eperon, J. A. Alexander-Webber, A. Abate, A. Sadhanala, S. Yao, Y. Chen, R. H. Friend, L. A. Estroff, U. Wiesner and H. J. Snaith, *Nat. Commun.*, 2015, 6, 6142.
43. W. Tress, N. Marinova, T. Moehl, S. M. Zakeeruddin, M. K. Nazeeruddin and M. Grätzel, *Energy Environ. Sci.*, 2015.
44. Y. Shao, Z. Xiao, C. Bi, Y. Yuan and J. Huang, *Nat. Commun.*, 2014, 5, 5784.

RSC Advances Accepted Manuscript